RESEARCH PAPER

The Structural, Electric and Dielectric Properties of $Ni_{0.7}Cd_{0.3}Nd_xFe_{2-x}O_4$ (0≤x≤0.03) Ferrite Prepared via Oxalate Co-Precipitation Route

Surekha S. Jadhav[1], Amit A. Bagade[2], Tukaram J. Shinde[3], Kesu Y. Rajpure[4,*]

* rajpure@yahoo.com

[1] Department of Physics, Annasaheb Dange College of Engineering & Technology, Ashta- 416 301, India

[2] Sharad Institute of Technology College of Engineering Yadrav, Ichalkaranji- 416121, India

[3] Department of Physics, KRP Kanya Mahavidyalaya, Islampur- 415409, India

[4] Electrochemical Materials Laboratory, Department of Physics, Shivaji University, Kolhapur- 416 004, India

Abstract: In present work $Ni_{0.7}Cd_{0.3}Nd_xFe_{2-x}O_4$ ferrite samples (0≤x≤0.03) were prepared by using oxalate co-precipitation technique. The different characterization techniques were utilized including X-ray diffraction (XRD), FT-infrared (FTIR) spectroscopy, scanning electron microscopy (SEM), DC electrical resistivity and dielectric measurements. The crystal structure, crystallite size, lattice constant, unit cell volume and theoretical density were systematically analysed. The XRD and FT-IR measurements confirmed the formation of single phase spinel ferrite structure. The cation distribution among the octahedral and tetrahedral sites were proposed on the basis of analysis of XRD patterns by employing Rietveld refinement analysis. The samples exist as a mixed type spinel with cubic structure. The DC electrical resistivity confirms the semiconducting behaviour and the Curie temperature decreased with the increase in Nd^{3+} content. The dielectric constant and loss tangent decreased with frequency and at higher frequencies remained constant, which shows the usual dielectric dispersion due to space charge polarization. The AC conductivity reveals that the small type polarons are responsible for conduction process.

Keywords: Oxalate Co-precipitation, Ni-Cd Ferrite, XRD, SEM, DC resistivity, Dielectric properties.

1. INTRODUCTION

The Ni–Cd ferrites are widely used in high-frequency devices due to it possesses low coercive field and high resistivity [1]. In last few years, synthesis and application of Ni-Cd ferrites is applied for research because of their unique electric and dielectric properties. The ferrite materials are extensively used as inductors, memory devices, high frequency devices and alternative future materials for water purification [2-4]. As far as concerned the high performance of spinel ferrite material the highly pure, nanocrystalline, and uniform particles are essential [2]. The physicochemical properties of the Ni-Cd ferrites are depend on the method of preparation, stoichiometry, sintering temperature/time, etc [5]. Several researchers have prepared ferrites material by various method viz., sol-gel [6], micro-emulsion [7], co-precipitation [8], citrate precursor [9], tartrate precursor [10], hydrothermal [11], high energy ball milling [12] and levitation-jet synthesis (LJS) [13]. Both structural and electrical properties are tailored by introducing small amount of rare earth element in nickel ferrite. The rare earth elements play an important role in determining the electric and

magnetic properties of ferrite [14]. Karanjkar et al. [15] studied the structural, Mossbauer and electrical properties of Ni-Cd ferrites by the ceramic method. The lattice parameter dependence on Cd content also Neel's two sub lattice models govern the behaviour of these ferrites up to about x= 0.2 and after that triangular spin prevails. Rahimi et al. [16] synthesized the Cd substituted nickel ferrite nanoparticles by employing the sol– gel auto-combustion method and studied the structural and magnetic behaviour. The magnetic properties of the nanoparticles shows increasing trend of saturation magnetization, while for x= 0.3 composition maximum value of saturation magnetization and low coercive field with increase in Cd substitution was observed. Also the magnetic moment of the samples linearly increased with Cd content in nickel ferrite.

In the present work, structural and morphological behaviour of Nd^{3+} substituted nickel cadmium ferrite prepared by oxalate co-precipitation method using sulphates as starting materials has been discussed. The prepared samples were characterized by XRD, FTIR, SEM, DC electrical resistivity and dielectric measurements. The Rietveld analysis of XRD patterns of Nd^{3+}

substituted Ni-Cd ferrite system has been discussed. The aim of Rietveld analysis is (i) to characterize the samples in terms of micro structural parameters such as unit cell volume, lattice constant and oxygen position parameters etc., and (ii) to estimate the cation distribution among tetrahedral-A and octahedral-B sites in the spinel lattice. In the present study the electric and dielectric properties of Nd^{3+} substituted nickel cadmium ferrite are studied as a function of composition and frequency.

2. EXPERIMENTAL PROCEDURES

2.1. Preparation of $Ni_{0.7}Cd_{0.3}Nd_xFe_{2-x}O_4$

Neodymium substituted nickel cadmium ferrite $Ni_{0.7}Cd_{0.3}Nd_xFe_{2-x}O_4$ (0≤x≤0.03) have been synthesized by oxalate co-precipitation route using a $NiSO_4 \cdot 6H_2O$, $CdSO_4 \cdot 7H_2O$, $FeSO_4.5H_2O$ mixed in the required stoichiometric ratios in double distilled water. The mixture was heated at 80°C for 3 h. Added ammonium oxalate solution with stirring until whole precipitation process is completed. After that filter the precipitate and wash it to 4 to 5 times. The precipitate was then allowed to dry at 100°C temperature. Pre-sintering of all the samples were carried out at 600°C for 2 h and sintering were carried out at 1000°C for 4 h. The presintered powder was milled in an agate mortar with AR grade acetone as a base and pressed in the form of pellets at pressure of 6 tones cm^{-2} for 10 min by using hydraulic pressure machine. 3 wt% Polyvinyl alcohol (PVA) was used as a binder. The size of pellets was 1.5 cm diameter. The pellets were finally sintered at 1000°C for 5 h in air followed by slow cooling in the furnace at room temperature to reduce porosity and increase density.

Role of pre-sintering: The purpose of pre-sintering is to decompose the oxalates, carbonates and higher oxides thereby reducing the evolution of gases during final sintering. This process helps to homogenize the material and control the shrinkage that occurs in the final sintering.

Sintering: Sintering involves large scale diffusion and erasing of the gradients of chemical potentials, resulting in the formation of the final product.

Third time sintering: The final stage of sintering involves heating of pelletized sample to a high temperature in air or oxygen. In this stage, the rate of sintering must be controlled as it affects the electrical as well as magnetic properties of ferrites. For good quality ferrites, the grain size should be uniform. The final sintering process achieves intergranular pores, continuous grain growth and develops microstructure. The samples sintered at 1000°C have further used for studying structural and electrical properties.

2.2. Experimental techniques used for characterization

The structural properties of $Ni_{0.7}Cd_{0.3}Nd_xFe_{2-x}O_4$ system were studied by a Bruker D2-Phaser X-ray powder diffractometer using Cu-Kα radiation (λ= 1.5406 Å). X-ray diffraction patterns were analyzed with the help of FullProf program by employing Rietveld refinement technique. The XRD patterns for all the samples were refined using the F d -3 m space group. The quality of fitting experimental data was assessed by calculating the parameters such as the 'goodness of fit' χ^2 and the R factors. The surface morphology of the samples was investigated using a JEOL JSM- 6360 scanning electron microscope (SEM). FTIR spectra were obtained using Perkin Elmer spectrophotometer in the range 200- 800 cm^{-1} in the KBr medium. The DC electrical resistivity of $Ni_{0.7}Cd_{0.3}Nd_xFe_{2-x}O_4$ system was measured by using the two probe method as a function of temperature with a high sensitive Keithley electrometer model- 6514. The dielectric measurements of $Ni_{0.7}Cd_{0.3}Nd_xFe_{2-x}O_4$ system was carried out using a high precision LCR meter bridge (HP-6284A) in the frequency range 20 Hz to 1 MHz. The AC conductivity of the samples was calculated from the dielectric measurements data.

3. RESULTS AND DISCUSSION

3.1. Structural analysis

The XRD patterns along with Rietveld refined data of $Ni_{0.7}Cd_{0.3}Nd_xFe_{2-x}O_4$ (0≤x≤0.03) ferrite system is shown in Fig. 2. All the diffraction peaks indicates the formation of pure single phase nickel cadmium ferrite. In the Rietveld refined XRD patterns the Bragg's peak positions are shown in vertical lines. The open circles indicate observed intensity; solid line represents Rietveld refined calculated intensity and the bottom line shows the difference between the observed and refined calculated intensities.
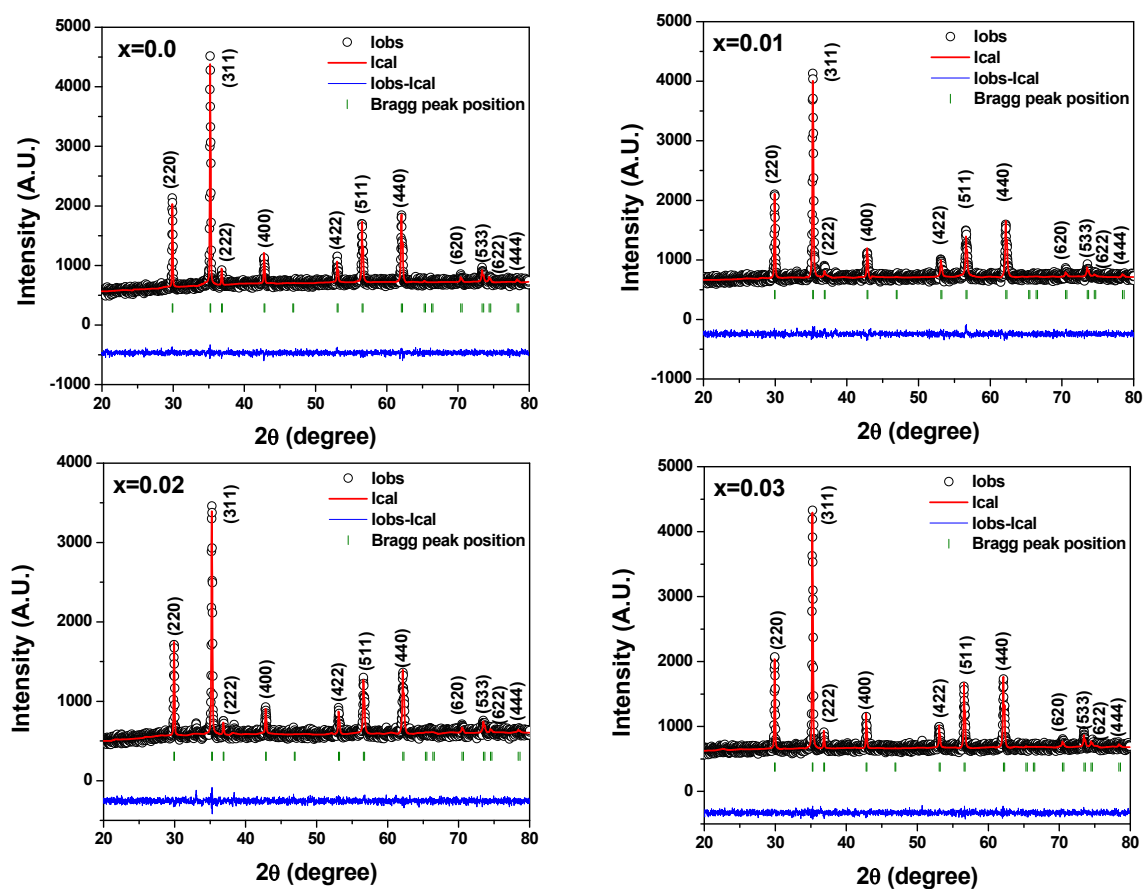
Fig. 1. Rietveld refined X-ray diffraction patterns of Ni$_{0.7}$Cd$_{0.3}$Nd$_x$Fe$_{2-x}$O$_4$ (0≤x≤0.03) ferrite system.
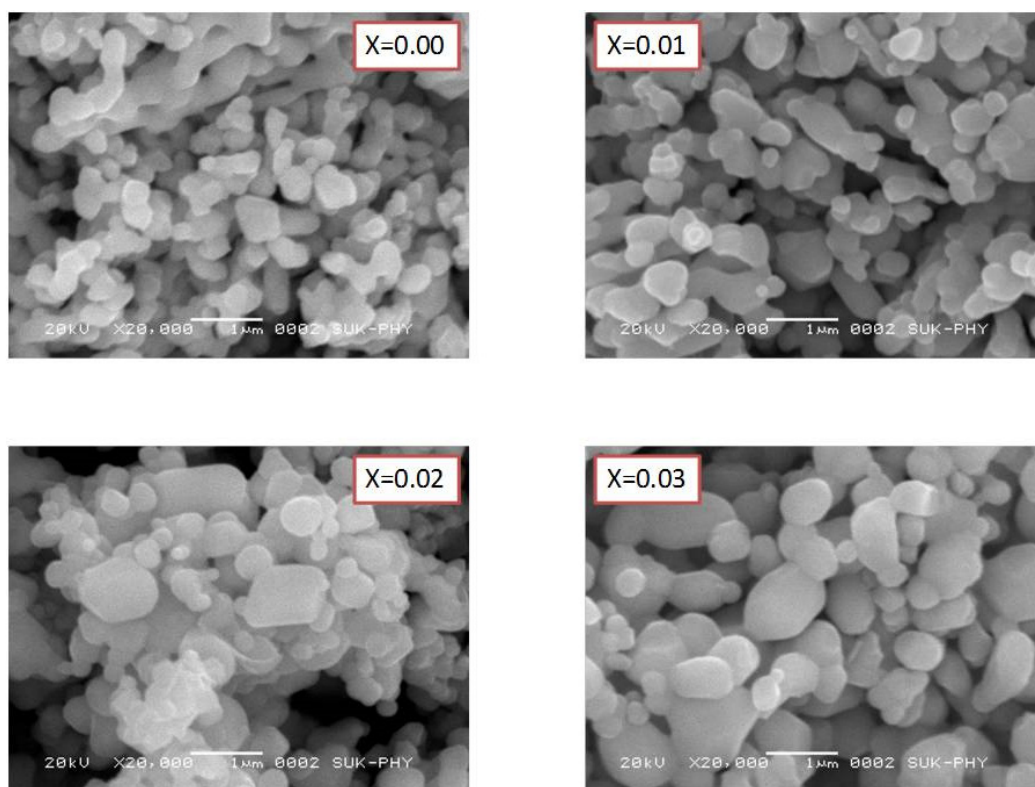
Fig. 2. Scanning electron microscopy images of Ni$_{0.7}$Cd$_{0.3}$Nd$_x$Fe$_{2-x}$O$_4$ (0≤x≤0.03) ferrite system.

The presence of major lattice planes (220), (311), (222), (400), (422), (511), (440) and (533) in the Rietveld refined patterns confirms the formation of spinel cubic crystal structure with no extra diffraction peaks. In the refinement, the oxygen positions (x=y=z) have been taken as free parameters and atomic fractional positions have been taken as fixed parameter. Other parameters such as lattice constants, temperature parameters, occupancies, scale factors, and shape parameters have been taken as free parameters. The quality of the Rietveld refinement was quantified by the corresponding figures of merit: Rwp and goodness of fit (χ^2). The background of the XRD pattern was corrected by Pseudo-Voigt function. The atomic coordinates (x, y, z) and occupancies of different atoms of $Ni_{0.7}Cd_{0.3}Nd_xFe_{2-x}O_4$ ($0 \leq x \leq 0.03$) are presented in Table 1. The values of 'goodness of fit (χ^2)' lies between 1 to 1.5 which indicating goodness of fitting. The Rietveld refined factors such as, χ^2,

R_{wp}, Re_{xp}, R_B, R_F, D, a, and ρ are summarized in Table 2. Based on these Rietveld refinements, the average crystallite sizes (D) is calculated using Scherer formula [1] and presented in Table 2. It is seen that the crystallite size of the samples varies from 52 to 58 nm with Nd^{3+} content. The similar effect of Nd^{3+} substitution in nickel ferrite was reported by Shinde et al. [17]. The cation distribution along with tetrahedral and octahedral interstitial sites is estimated using the Rietveld refinement analysis of the occupancy values. The estimated cation distribution with the ionic radius of the tetrahedral (r_A) and octahedral [r_B] sites of $Ni_{0.7}Cd_{0.3}Nd_xFe_{2-x}O_4$ ($0 \leq x \leq 0.03$) have listed in Table 3. The cation distribution of the two sites in the spinel lattice can be expressed as: $(Ni_{0.7}Fe_{0.3})_A[Nd_xFe_{2-x}]_BO_4$, where round bracket represents occupied tetrahedral sites (A-site) and square brackets represent occupied octahedral sites (B-site).

Table 1. Position coordinates and different atoms occupancies of $Ni_{0.7}Cd_{0.3}Nd_xFe_{2-x}O_4$ ($0 \leq x \leq 0.03$) ferrite system.

Spinel lattice sites	Atom	Position coordinates			Occupancy			
		x	y	z	X= 0.0	X= 0.01	X= 0.02	X= 0.03
Tetrahedral (A-site)	Ni	0.125	0.125	0.125	0.7	0.7	0.7	0.7
	Cd	0.125	0.125	0.125	0.3	0.3	0.3	0.3
Octahedral (B-site)	Fe	0.500	0.500	0.500	2.0	1.99	1.98	1.97
	Nd	0.500	0.500	0.500	--	0.01	0.02	0.03

Table 2. Rietveld refinement factors of $Ni_{0.7}Cd_{0.3}Nd_xFe_{2-x}O_4$ ($0 \leq x \leq 0.03$) ferrite system.

Rietveld refinement factors	Nd, content			
	X= 0.0	X= 0.01	X= 0.02	X= 0.03
$\chi 2$	1.04	1.17	1.02	1.05
R_B (%)	2.78	2.51	2.66	2.76
R_F (%)	3.49	2.98	3.19	4.32
Rwp	17.7	26.6	27.6	25.3
Rexp	17.3	24.6	27.3	24.6
D (nm)	52	54	55	58
a (Å)	8.4433	8.4437	8.4445	8.4460
V (a^3)	604.06	601.35	601.98	602.48
ρ (g/cm³)	6.551	6.711	6.205	6.765
Oxygen position (x=y=z)	0.2596	0.2588	0.2541	0.2596

Table 3. Cation distribution occupancy with Bond length (R_A and R_B) and ionic radius (r_A and r_B) of the tetrahedral and octahedral sites of $Ni_{0.7}Cd_{0.3}Nd_xFe_{2-x}O_4$ ($0 \leq x \leq 0.03$) ferrite system.

Sr. No.	Nd, content (x)	Cation distribution	R_A (Å)	R_B (Å)	r_a (Å)	r_B (Å)
1	0.00	$(Ni_{0.7}Cd_{0.3})_A[Fe_2]_BO_4$	1.9180	2.063	0.5680	0.7126
2	0.01	$(Ni_{0.7}Cd_{0.3})_A[Nd_{0.01}Fe_{1.99}]_BO_4$	1.9151	2.060	0.5651	0.7095
3	0.02	$(Ni_{0.7}Cd_{0.3})_A[Nd_{0.02}Fe_{1.98}]_BO_4$	1.9158	2.061	0.5658	0.7102
4	0.03	$(Ni_{0.7}Cd_{0.3})_A[Nd_{0.03}Fe_{1.97}]_BO_4$	1.9163	2.062	0.5663	0.7108

The Bond length and the ionic radii of the tetrahedral (A) and octahedral [B] sites respectively can be calculated by using following equation, [18]

$$R_A = a\sqrt{3}\left(\delta + \frac{1}{8}\right) \quad \text{and} \quad R_B = a\left(3\delta + \frac{1}{16} - \frac{\delta}{2}\right)^{1/2} \quad (1)$$

$$r_A = a\sqrt{3}\left(u - \frac{1}{4}\right) - r_0 \quad \text{and} \quad r_B = a\left(\frac{5}{8} - u\right) - r_0 \quad (2)$$

where, R_A and R_B are the bond lengths of tetrahedral and octahedral sites, r_A and r_B are the ionic radii of tetrahedral and octahedral sites, 'u' the oxygen position parameter (u= 0.381) and r_o is the radius of the oxygen ions (r_o= 1.32 Å). The Bond lengths RA, RB and ionic radius r_A, r_B of A-site and B-site are increasing linearly due to the increase in lattice constant with increasing Nd^{3+} content.

3.2. Scanning electron microscopy

Figure 2 shows the SEM micrographs of $Ni_{0.7}Cd_{0.3}Nd_xFe_{2-x}O_4$ (0≤x≤0.03) ferrite system. The micrographs show the agglomerated grain structure with clusters of fine particles sticking together. The morphology of samples is almost uniform and spherical having cubical to nearly spherical shaped particles. Uniform nature of the grains is revealed with some agglomeration. The average grain size is varied with Nd^{3+} content and calculated by line intercept method. The grain size increases with increase in Nd^{3+} content in nickel cadmium ferrite. The average grain size of prepared samples is about 630 nm. The grain size of the sample prepared at x= 0.03 composition is relatively higher than other samples due maximum Fe^{3+} ions are occupied by Nd^{3+} ions and ionic radius of Nd^{3+} is larger than Fe^{3+} ions. It is also seen that the size of the grains increases with decreasing the area of grain boundary. The increase in pores, vacancies and scattering centres for electrical charge carries confirm the dispersion of Nd^{3+} in the ferrite system. The variation in the grain size with Nd^{3+} content is due to the method of synthesis as well as mechanically induced contraction and the deformation of Fe^{2+}-O^{2-}-Fe^{3+} bonds [19].

3.3. DC electrical resistivity

The variation of DC electrical resistivity (logρ) against reciprocal of temperature (1000/T) for $Ni_{0.7}Cd_{0.3}Nd_xFe_{2-x}O_4$ (0≤x≤0.03) ferrite system is shown in Fig. 3. It is seen that the electrical resistivity of all the samples decreases with

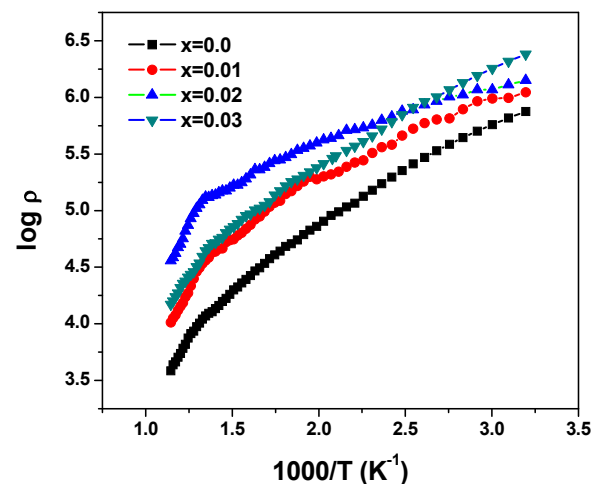increasing temperature, indicating the semiconducting behavior of ferrite samples.

Fig. 3. Variation in DC electrical resistivity with temperature of $Ni_{0.7}Cd_{0.3}Nd_xFe_{2-x}O_4$ (0≤x≤0.03) ferrite system.

The basic Ni-Cd ferrite was considered to be a high resistive spinel ferrite material [20]. The DC resistivity could be further increased by doping with rare earth ion and the preference of the occupying ion to fill the interstitial sites of spinel lattice. The decrease in resistivity with increase in temperature is due to increase in the thermally activated drift mobility of charge carriers, according to the charge hopping conduction mechanism [21]. The activation energy of all the ferrite samples was calculated by using the Arrhenius relation [22],

$$\rho = \rho_0 \exp\left(\frac{\Delta E}{KT}\right) \quad (3)$$

where, ρ is the resistivity, ΔE is the activation energy, k is the Boltzmann constant, T is the absolute temperature and ρ_0 temperature dependent constant. The resistivity plots show the two regions corresponding to two phases. At lower temperature the first region is observed due to the ordered state of ferromagnetic nature and at higher temperature the second region is observed due to relatively disordered paramagnetic nature and electron hopping [23]. The first region is a ferromagnetic region with a break at Curie temperature (Tc) and second region is a paramagnetic region at higher temperature. The electrons can transfer from one lattice site to another by getting the required activation energy in electron hopping mechanism. The activation energy was estimated in ferromagnetic and

paramagnetic regions. The values of the activation energies for both ferromagnetic and paramagnetic regions are presented in Table 4. The activation energies of ferromagnetic region are higher than paramagnetic region due to disordered states of the ferromagnetic region and the ordered states of the paramagnetic region [24]. Said et al. [25] reported similar behavior for Sm^{3+} substituted Ni-Cd ferrites. The Curie temperature (Tc) decreases with increase in Nd^{3+} content in Ni-Cd ferrite. It is also seen that the resistivity of Nd3+ substituted Ni-Cd ferrite is larger than pure Ni-Cd ferrite. It is attributed to the increasing average grain size with increase in Nd^{3+} content. The small grains imply larger number of insulating grain boundaries and hence the greater energy barriers to electron conduction, resulting in higher electrical resistivity [26]. Hamdaoui et al. [27] studied the electrical conductivity of Ni-Cd ferrite, the activation energy varies with varying Cd content and very close to current work. Rashed et al. [28] prepared Li-Cd doped cobalt ferrite by hydrothermal method and the electrical resistivity increases with increase in dopant concentration from 2.8×10^7 ohm.cm to 7.3×10^7 ohm.cm due to replacement of Li^{1+} to Fe^{3+} ions on octahedral site. Prasad et al, [29] studied the DC electrical resistivity of Cd substituted Ni-Zn ferrite, he showed that the resistivity increases upto x= 0.12 and then decreases due to combined consequence of the site occupancy of Cd^{2+} ions and the partial volatilization of cadmium leading to the formation of Fe^{2+} ions, also activation energy varies in the range 0.18- 0.55 with Cd content.

3.4. FTIR studies

The FTIR absorption spectra of $Ni_{0.7}Cd_{0.3}Nd_xFe_{2-x}O_4$ ($0 \leq x \leq 0.03$) ferrite system are shown in Fig. 4. The spectra show two characteristic absorption bands in the range of 400- 600 cm^{-1}. The higher

wave number absorption band υ1 is in the range of 590– 599 cm^{-1} and the lower wave number absorption band υ2 is in the range of 397– 403 cm^{-1}. First band, at about 600 cm^{-1} (υ1), is attributed to the intrinsic stretching vibration of the tetrahedral metal- oxygen bond and second one at about 400 cm^{-1} (υ2), which is attributed to the intrinsic stretching vibration of the octahedral metal- oxygen bond. The position of the characteristic band depends on the lattice vibrations involving tetrahedral (A-site) and octahedral (B-site) metal ions present in the spinel lattice. The presence of two absorption bands is a common observation made by many other researchers for spinel ferrite [30, 31]. The band positions Nd^{3+} substituted Ni-Cd ferrite are presented in Table 4. It is seen that the band υ2 shifts slightly to higher wavenumber side with increase in Nd^{3+} content. Similar type of variation in band positions is reported by Sabikoglu et al. [32] for Nd^{3+} substituted nickel ferrite. The shifts in the bands υ1 and υ2 are due to the disorder occurring between Fe^{3+}- O^{2-} bond by substituting Nd^{3+} ions.
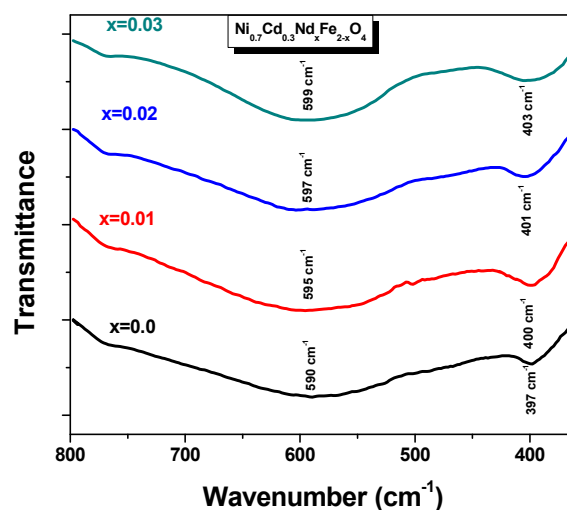

Fig. 4. FTIR absorption spectra of $Ni_{0.7}Cd_{0.3}Nd_xFe_{2-x}O_4$ ($0 \leq x \leq 0.03$) ferrite system.

Table 4. Curie temperatures and activation energies of $Ni_{0.7}Cd_{0.3}Nd_xFe_{2-x}O_4$ ($0 \leq x \leq 0.03$) ferrite system.

Nd, content, (x)	Activation energy, ΔE (eV)		Curie temperature Tc (ºC)	Absorption bands (cm^{-1})	
	Paramagnetic region	Ferromagnetic region		υ1	υ2
0.00	0.41	0.23	530	590	397
0.01	0.44	0.32	518	595	400
0.02	0.42	0.29	512	597	401
0.03	0.63	0.39	505	599	403

3.5. Dielectric properties

3.5.1. *Dielectric constant and loss tangent*

The effect of Nd^{3+} substitution on the dielectric properties of $Ni_{0.7}Cd_{0.3}Nd_xFe_{2-x}O_4$ ($0 \leq x \leq 0.03$) ferrite system has been studied. The real part of the dielectric constant (ε') is calculated by using equation [33],

$$\varepsilon' = \frac{Ct}{\varepsilon_0 A} \tag{4}$$

where, C is the capacitance, 't' the thickness of the pellet, 'A' the area of cross section, ε_0 the permittivity of free space (8.85×10^{-14} F/m). The frequency dependant real part of the dielectric constant of the $Ni_{0.7}Cd_{0.3}Nd_xFe_{2-x}O_4$ ($0 \leq x \leq 0.03$) ferrite system is shown in Fig. 5. It is seen that at the low frequency side real part of the dielectric constant (ε') slowly decreases and at higher frequency side it is constant due to at a certain frequency electric charge cannot follow the changes of applied electric field. In Nd^{3+} substituted Ni-Cd ferrite, the Nd^{3+} ions present in the octahedral B-site is responsible for reductions in concentration of Fe^{3+} ions in octahedral B-site which reduces the movement of Fe^{2+} to Fe^{3+}. Therefore real part of dielectric constant decreases with increase in frequency and attains a constant value at higher frequency. The relative dielectric constant and loss tangent at x=0.0 is high and decreases with an increase in the Nd^{3+} content.
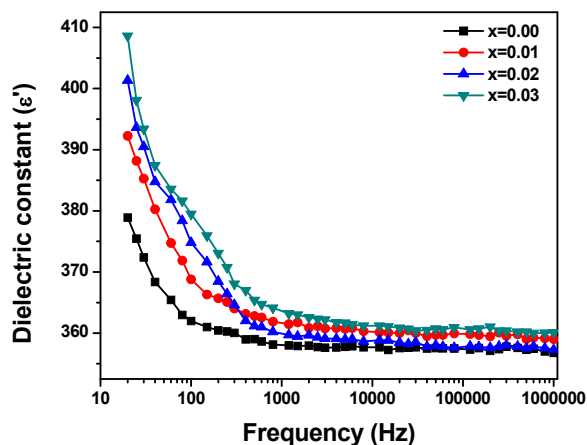

Fig. 5. Frequency dependant dielectric constant (ε') for $Ni_{0.7}Cd_{0.3}Nd_xFe_{2-x}O_4$ ($0 \leq x \leq 0.03$) ferrite system.

In the present investigation the substitution of Nd^{3+} in the B-site may decrease the concentration of Fe^{3+} ion. From Fig. 5 it is seen that the substitution of Nd^{3+} rare earth ions at the Fe^{3+} ions

the values of the ε' increases with increase in Nd^{3+} content due to decrease in the number of Fe^{3+} ions in B-site [34]. The room temperature variation in loss tangent ($\tan\delta$) with frequency of $Ni_{0.7}Cd_{0.3}Nd_xFe_{2-x}O_4$ ($0 \leq x \leq 0.03$) ferrite system is shown in Fig. 6. It is seen that at lower frequencies higher loss tangent is observed and then decreases slowly with increasing frequency. This dielectric dispersion type of interfacial polarization is attributed to the Maxwell-Wagner type [35]. The decrease in dielectric loss tangent with change in frequency is based on the with Koop's phenomenological theory [36].
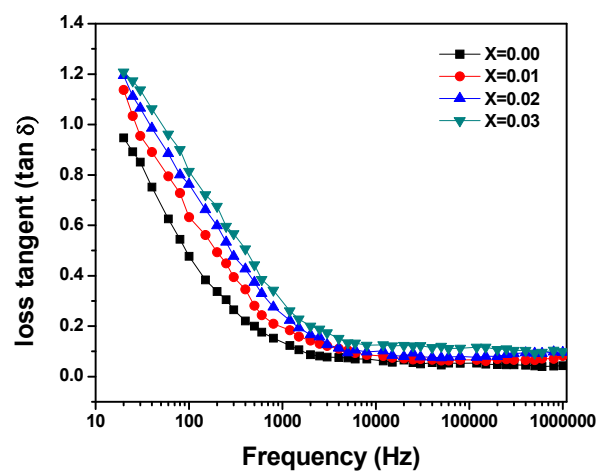

Fig. 6. Variations in loss tangent ($\tan\delta$) with frequency of $Ni_{0.7}Cd_{0.3}Nd_xFe_{2-x}O_4$ ($0 \leq x \leq 0.03$) ferrite system.

3.5.2. *AC conductivity study*

The AC conductivity (σ_{ac}) of $Ni_{0.7}Cd_{0.3}Nd_xFe_{2-x}O_4$ ($0 \leq x \leq 0.03$) ferrite system is calculated using dielectric parameters and is given by relation [22],

$$\sigma_{ac} = \omega\varepsilon'\varepsilon_0\tan\delta \tag{5}$$

where, ω is the angular frequency and $\tan\delta$ the loss tangent.

The room temperature AC conductivity with respect to angular frequency (ω) is shown in Fig.7. The values of AC conductivity slightly changes due very slight variation of the stoichiometry. The ac conductivity takes place by jump phenomena of charge carriers between defect states in the energy bands. We notice the decrease of the ac conductivity when the frequency increases. This behaviour is due to the effect of the frequency which increases the area of space charges. From this graph it is clear that, the AC conductivity of samples increases with increase in angular frequency (ω) which indicates

that the conduction mechanism is due to very small interaction of electrons and atoms called as polarons. According to this interaction they are classified two types i.e. small polarons and large polarons. In case of small polarons, the AC conductivity increases with angular frequency (ω) and in case of large polarons conductivity decreases with an increase in frequency [37]. Therefore from this plot we have seen that small polarons is responsible for increasing conductivity of $Ni_{0.7}Cd_{0.3}Nd_xFe_{2-x}O_4$ ($0\leq x\leq 0.03$) ferrite system. From this graph it is seen that at certain frequencies conductivity decreases due to mixed polarons (small and large). The AC conductivity increases gradually at low frequency, and increases sharply at high frequencies. From this study it conclude that conduction of ferrite is due to electron hoping between Fe^{2+}-Fe^{3+} ions on octahedral site [38].
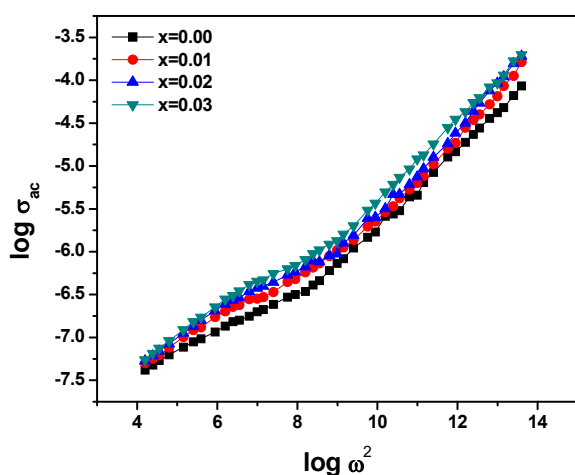

Fig. 7. Variation in AC conductivity of $Ni_{0.7}Cd_{0.3}Nd_xFe_{2-x}O_4$ ($0\leq x\leq 0.03$) ferrite system.

4. CONCLUSIONS

The oxalate co-precipitation technique was employed to synthesize $Ni_{0.7}Cd_{0.3}Nd_xFe_{2-x}O_4$ ($0\leq x\leq 0.03$) ferrite series. Rietveld refinement prediction confirmed the formation of pure single phase nickel cadmium ferrite. The lattice constant and crystallite size increased with the increase in Nd^{3+} content and resistivity results showed the semiconducting behaviour of $Ni_{0.7}Cd_{0.3}Fe_{2-x}O_4$ ferrite. The micrographs showed the agglomerated grain structure with clusters of fine particles sticking together and the grain size varied with Nd^{3+} content. The activation energies of ferromagnetic region were higher than

paramagnetic regions and Curie temperature (Tc) decreased from 530 to 505°C with the increase in Nd^{3+} content. The dielectric measurement revealed the usual dielectric dispersion due to space charge polarization. The AC conductivity indicated that the small polarons have contributed for conduction process.

REFERENCES

[1] Coutinho, D.M. and Verenkar, V.M.S., "Spin canting and surface spin disorder in Ni substituted Co-Cd ferrite nanoparticles synthesized by fuel deficient combustion method." J. Alloys Compd., 2019, 782, 392-403.

[2] Dongale, T.D., Khot, S.S., Khot, Patil, A.A., Wagh, S.V., Wagh, Patil, P.B, Dubal, D.P. and T. G. Kim, "Bifunctional nanoparticulated nickel ferrite thin films: Resistive memory and aqueous battery applications." Mater. Des., 2021, 201, 109493.

[3] Wu, X.H., Li, L.Z., Wu, B., Zhong, X.X., Wang, R., Tu, X.Q., He, L. and Wang, F.H. "Structural, magnetic and electrical properties of $K_{0.5}Na_{0.5}NbO_3$ doped NiZnCo ferrite for high frequency device." J. Eur. Ceram. Soc., 2020, 40, 1301-1306.

[4] Shakila, M., Inayata, U., Khalid, N.R., Tanveer, M., Gillani, S.S.A., Tariq, N.H., Shah, A., Mahmood, A., Dahshan, A. "Enhanced structural, optical, and photocatalytic activities of Cd–Co doped Zn ferrites for degrading methyl orange dye under irradiation by visible light." J. Phys. Chem. Solids., 2022, 161, 110419.

[5] Verma, R., Kane, S.N., Deshpande, U.P. and Mazaleyrat, F. "Impact of Cd content on properties of $Ni_{1-x}Cd_xFe_2O_4$ nanoferrites prepared without post-preparation thermal treatment." Mater. Today: Proc., 2021, 46, 2205-2211.

[6] Jasrotia, R., Puri, P., Verma, A. and Singh V. P. "Magnetic and electrical traits of sol-gel synthesized Ni-Cu-Zn nanosized spinel ferrites for multi-layer chip inductors application." J. Solid State Chem., 2020, 289, 121462.

[7] Khan, M.A., Zaman, M.Q., Majeed, A., Akhtar, M.N. and Abbas, W. "Structural, spectral, dielectric and magnetic properties

of $Sr_2Cu_xNi_{2-x}Fe_{28-x}Cr_xO_{46}$ $(0 \leq x \geq 0.5)$ ferrites synthesized via micro-emulsion route." Mater. Chem. Phys., 2021, 259, 124066.

[8] Vigneswari, T. and Raji, P. "Structural and magnetic properties of calcium doped nickel ferrite nanoparticles by co-precipitation method." J. Mol. Struct., 2017, 1127, 515-521.

[9] Verma, S., Chand, J. and Singh, M. "Structural and electrical properties of Al^{3+} ions doped nanocrystalline $Mg_{0.2}Mn_{0.5}Ni_{0.3}Al_yFe_{2-y}O_4$ ferrites synthesized by citrate precursor method." J. Alloys Compd., 2014, 587, 763-770.

[10] Yang, J.M. and Yen, F.S. "Evolution of intermediate phases in the synthesis of zinc ferrite nanopowders prepared by the tartrate precursor method." J. Alloys Compd., 2008, 450, 387-394.

[11] Majida, F., Rauf, J., Ata, S., Bibi, I., Malik, A., Ibrahim, S.M., Ali, A. and Iqbal, M. "Synthesis and characterization of $NiFe_2O_4$ ferrite: Sol–gel and hydrothermal synthesis routes effect on magnetic, structural and dielectric characteristics." Mater. Chem. Phys., 2021, 258, 123888.

[12] Yuan, Z., Chen, Z-H., Chen, D. and Kang, Z-T. "Analyses of factors affecting nickel ferrite nanoparticles synthesis in ultrasound-assisted aqueous solution ball milling." Ultrason. Sonochem., 2015, 22, 188-197.

[13] Hernández, P.T., Kuznetsov, M.V., Morozov, I.G. and Parkin, I.P. "Application of levitation-jet synthesized nickel-based nanoparticles for gas sensing." Mater. Sci. Eng. B., 2019, 244, 81-92.

[14] Hirosawa, F. and Iwasaki, T. A. "Comparative study of the magnetic induction heating properties of rare earth (RE= Y, La, Ce, Pr, Nd, Gd and Yb)-substituted magnesium–zinc ferrites." Solid State Sci., 2021, 118, 106655.

[15] Karanjkar, M.M., Tarwal, N.L., Vaigankar, A.S. and Patil, P.S. "Structural, Mossbauer and electrical properties of nickel cadmium ferrites." Ceram. Int., 2013, 39, 1757-1764.

[16] Rahimi, M., Eshraghi, M. and Kameli, P. "Structural and magnetic characterizations of Cd substituted nickel ferrite nanoparticles." Ceram. Int., 2014, 40, 15569-15575.

[17] Shinde, T.J., Gadkari, A.B. and Vasambekar, P.N. "Influence of Nd^{3+} substitution on structural, electrical and magnetic properties of nanocrystalline nickel ferrites." J. Alloys Compd., 2012, 513, 80-85.

[18] Sawant V.S. and Rajpure, K.Y. "The effect of Co substitution on the structural and magnetic properties of lithium ferrite synthesized by an autocombustion method." J. Magn. Magn. Mater., 2015, 382, 152-157.

[19] Kobylinska, A., Kniec, K., Maciejewska, K. and Marciniak, L. "The influence of dopant concentration and grain size on the ability for temperature sensing using nanocrystalline $MgAl_2O_4$: Co^{2+}, Nd^{3+} luminescent thermometers." New J. Chem., 2019, 43, 6080.

[20] Shelar, M.B., Jadhav, P.A., Chougule, S.S., Mallapur, M.M. and Chougule, B.K. "Structural and electrical properties of nickel cadmium ferrites prepared through self-propagating auto combustion method." J. Alloys Compd., 2009, 476, 760-764.

[21] Patil, D.R. and Chougule, B.K. "Effect of resistivity on magnetoelectric effect in $(x)NiFe_2O_4–(1-x)Ba_{0.9}Sr_{0.1}TiO_3$ ME composites." J. Alloys Compd., 2009, 470, 531-535.

[22] Bagade, A.A. and Rajpure, K.Y. "Studies on NO_2 gas sensing properties of sprayed $Co_{1-x}Mn_xFe_2O_4$ $(0 \leq x \leq 0.5)$ spinel ferrite thin films." Ceram. Int., 41 (2015) 7394-7401.

[23] Sawant, V.S., Shinde, S.S., Deokate, R.J., Bhosale, C.H., Chougule, B.K. and Rajpure, K.Y. "Effect of calcining temperature on electrical and dielectric properties of cadmium stannate." Appl. Surf. Sci., 2009, 255, 6675-6678.

[24] Patil, M.R., Rendale, M.K., Mathad, S.N. and Pujar, R.B. "Electrical and magnetic properties of Cd^{2+} doped Ni-Zn ferrites." Inorg. Nano-Met. Chem., 2017, 47, 1145–1149.

[25] Said, M.Z., Hemeda, D.M., Kadar, S.A. and Farag, G.Z. "Structural, electrical and infrared studies of Ni_{0.7}Cd_{0.3}Sm_

xFe_{2-x}O_4 ferrite." Turk. J. Phys., 2007, 31, 41-50.

[26] Verma, A. and Dube, D.C. "Processing of nickel–zinc ferrites via the citrate precursor route for high-frequency applications." J. Am. Ceram. Soc., 2005, 88, 519-523.

[27] Hamdaoui, N., Azizian-Kalandaragh, Y., Khlifi, M. and Beji, L. "Cd-doping effect on morphologic, structural, magnetic and electrical properties of $Ni_{0.6-x}Cd_xMg_{0.4}Fe_2O_4$ spinel ferrite $(0 \leq x \leq 0.4)$." J. Alloys Compd., 2019, 803, 964-970.

[28] Rasheed, S., Khan, R.A., Shah, F., Ismail, B., Nisar, J., Shah, S.M., Rahim, A. and Khan, A.R. "Enhancement of Electrical and Magnetic Properties of cobalt ferrite nanoparticles by co-substitution of Li-Cd ions." J. Magn. Magn. Mater., 2019, 471, 236-241.

[29] Siva Ram Prasad, M., Prasad, B.B.V.S.V., Rajesh, B., Rao, K.H. and Ramesh, K.V. "Magnetic properties and DC electrical resistivity studies on cadmium substituted nickel–zinc ferrite system." J. Magn. Magn. Mater., 2011, 323, 2115-2121.

[30] Rao, P.A., Raghavendra, V., Suryanarayana, B., Paulos, T., Murali, N., Phanidhar Varma, P.V.S.K., Prasad, R.G., Ramakrishna, Y. and Chandramouli, K. "Cadmium substitution effect on structural, electrical and magnetic properties of Ni-Zn nano ferrites." Results Phys., 19 (2020) 103487.

[31] Borade, R.M., Somvanshi, S.B., Kale, S.B., Pawar, R.P. and Jadhav, K.M. "Spinel zinc ferrite nanoparticles: an active nanocatalyst for microwave irradiated solvent free synthesis of chalcones." Mater. Res. Express., 2020, 7, 016116.

[32] Sabikoglu, I., Parali, L., Malina, O., Novak, P., Kaslik, J., Tucek, J., Pechousek, J., Navarik, J. and Schneeweiss, O. "The effect of neodymium substitution on the structural and magnetic properties of nickel ferrite." Pro. Nat. SCI-Mater., 2015, 25, 215-221.

[33] Ikram, S., Jacob, J., Arshad, M.I., Mahmood, K., Ali, A., Sabir, N., Amin, N. and Hussain, S. "Tailoring the structural, magnetic and dielectric properties of Ni-Zn-CdFe$_2$O$_4$ spinel ferrites by the substitution of lanthanum ions." Ceram. Int., 2019, 45, 3563-3569.

[34] Shinde, T.J., Gadkari, A.B. and Vasambekar, P.N. "Effect of Nd^{3+} substitution on structural and electrical properties of nanocrystalline zinc ferrite." J. Magn. Magn. Mater., 2010, 322, 2777-2781.

[35] Hajlaoui, M.E., Dhahri, R., Hnainia, N., Benchaabane, A., Dhahri, E. and Khirouni, K. "Dielectric spectroscopy study of the Ni$_{0.2}$Zn$_{0.8}$Fe$_2$O$_4$ spinel ferrite as a function of frequency and temperature." Mater. Sci. Eng. B., 2020, 262, 114683.

[36] Koops, C.G. "On the dispersion of resistivity and dielectric constant of some semiconductors at audio frequencies." Phys. Rev., 1951, 83, 121-124.

[37] Kumbhar, S.S., Mahadik, M.A., Mohite, V.S., Rajpure, K.Y., Kim, J.H. Moholkar, A.V. and Bhosale, C.H. "Structural, dielectric and magnetic properties of Ni substituted zinc ferrite." J. Magn. Magn. Mater., 2014, 363, 114-120.

[38] Arifuzzaman, M., Hossen, M.B., Afroze, J.D. and Abden, M.J. "Structural and electrical properties of Cu substituted Ni–Cd nanoferrites for microwave applications, Physica B Condens. Matter." 2020, 588, 412170.